Nuclear Spins in a Nanoscale Device for Quantum Information Processing

Ş. K. Özdemir,[1,2,3] A. Miranowicz,[1,3,4] T. Ota,[1,5] G. Yusa,[5,6,7] N. Imoto,[1,2,3] and Y. Hirayama[1,7]

[1]*SORST-JST, Honmachi, Kawaguchi, 331-0012 Saitama, Japan*
[2]*CREST-JST, Honmachi, Kawaguchi, 331-0012 Saitama Japan*
[3]*Graduate School of Engineering Science, Osaka University, 1-3 Machikaneyama, Toyonaka, 560-8531 Osaka, Japan*
[4]*Institute of Physics, Adam Mickiewicz University, 61-614 Poznań, Poland*
[5]*NTT Basic Research Labs, NTT Corporation, Atsugi, 243-0198 Kanagawa, Japan*
[6]*PRESTO-JST, Honmachi, Kawaguchi, 331-0012 Saitama, Japan*
[7]*Department of Physics, Tohoku University, Sendai, 980-8578 Miyagi, Japan*

Coherent oscillations between any two levels from four nuclear spin states of $I = 3/2$ have been demonstrated in a nanometre-scale NMR semiconductor device, where nuclear spins are all-electrically controlled. Using this device, we discuss quantum logic operations on two fictitious qubits of the $I = 3/2$ system, and propose a quantum state tomography scheme based on the measurement of longitudinal magnetization, M_z.

INTRODUCTION

It has long been demonstrated that nuclear spins have long relaxation times, thus longer coherence times, making them suitable for quantum information processing devices [1, 2] (for a review see [3] and references therein). Most of the works on the manipulation and use of nuclear spins are restricted to those in molecules of liquid solutions. To date, liquid-state NMR is the leader among all quantum computer implementations, both in the number of qubits controlled and the number of gates performed within the coherence lifetime. These successful demonstrations inspired researches to investigate the possibility to use NMR in solid-state systems for the same purpose [4]. Coherent manipulation of nuclear spins in solid-state systems became an exciting field of research which resulted in interesting proposals on nuclear spin qubits, where nuclear spins are individually manipulated [5, 6].

An advantage of solid-state NMR over the liquid NMR is that the spins can be highly polarized by dynamic nuclear spin polarization techniques such as polarization transfer from electronic spins. This strong polarization allows a large population available for the preparation of the system close to a pure state. However, only a few quantum information processing experiments with single-crystal solids have been reported [4, 7].

Most of the experiments up to date employ conventional NMR technique, which uses metal coils for excitation and detection of nuclear spin transverse-magnetization M_{xy}. In order to obtain a detectable signal, a large number of nuclear spins ($10^{11} - 10^{13}$) should be involved in the process, which limits the sensitivity of these schemes. Moreover, quantum multiple coherence is not directly detected in conventional NMR as it does not produce transverse magnetization.

In a recent study [8], Yusa *et al.* demonstrated an all-electrical control and detection of nuclear spin magnetization in a nanometre-scale semiconductor device, where longitudinal magnetization M_z of nuclear spins in a point-contact channel are detected by the resistivity change of the channel paving the way to the detection of multiple quantum coherence. This device has an improved sensitivity, which requires the involvement of only $\sim 10^8$ or less nuclear spins.

In the following, we first describe this nanoscale NMR device, the novel detection technique and the observed multiple quantum coherence. Then, we show how one- and two-qubit operations can be performed on this device, and give the pulse sequences. A method for performing quantum state tomography using M_z-detection in this device is also presented, and finally we give a brief discussion and conclusion.

NANOSCALE SEMICONDUCTOR NMR DEVICE

Principle of the device: The nanoscale NMR device is fabricated as a monolithic semiconductor device integrated with a point contact channel and an antenna gate (see Fig. 1). The structure contains a 20-nm GaAs quantum well with AlGaAs barrier layers grown on n-GaAs(100) substrate. This substrate functions as backgate to control the electron density in the point contact region, which is defined by split Schottky gates separated by 600nm. The antenna gate locally irradiates the channel with an alternating rf field for selective and coherent manipulation of the nuclear spins.

By controlling the static magnetic field perpendicular to the grown device surface and the backgate voltage, the point contact region was set to fractional quantum Hall regime at the degenerate Landau-level filling factor $\nu = 2/3$, where there is a strong coupling of nuclear spins to the conduction electrons [9, 10, 11]. At $\nu = 2/3$, the spin polarized and unpolarized states face each other through a transition region with high resistivity R_{xx}. When sufficient current is driven through the system, the polarized nuclear spins interact with the flowing electrons resulting in an gradual enhancement of

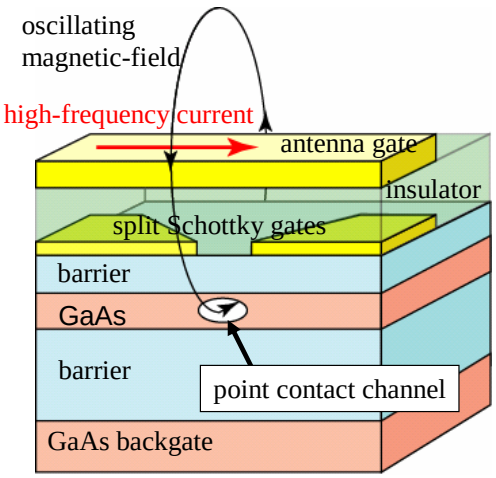

FIG. 1: Schematic diagram illustrating the semiconductor device for coherent-control of nuclear spins in a nanometre-scale region. The point contact channel, which is pointed with an arrow, is defined by a Schottky gate pair.

R_{xx}. Thus, the current density becomes very high in the constricted region so that nuclear spin polarization occurs only in the point contact region. This enhancement of R_{xx} implies that the polarization of the nuclear spins in the point contact region can be detected by measuring the resistance between the ends of the point contact. It has already been shown that this resistance values is proportional to the longitudinal magnetization of nuclear spins, $\Delta M_z \propto \Delta R_{xx}$ [10].

Observation of coherent oscillation with R_{xx} measurement: The point contact channel in this device consists of ^{69,71}Ga and ^{75}As isotopes each having total spin $I = 3/2$. Thus, each nuclide splits into $n = 2I+1 = 4$ energy states, $|m\rangle = |3/2\rangle, |1/2\rangle, |-1/2\rangle, |-3/2\rangle$, under static magnetic field due to Zeeman effect. This levels are spaced with equal energy separation of $\hbar\omega_0$. However, the quadrupolar interaction shifts the adjacent states by $2\Delta_q$ from $\hbar\omega_0$ allowing three possible transitions at resonances $\hbar\omega_0 - 2\Delta_q$, $\hbar\omega_0$ and $\hbar\omega_0 + 2\Delta_q$ (see Fig. 3). While these transitions are between levels separated by one quantum angular momentum ($\Delta m = 1$), energy and angular momentum conservation rules imply that transitions between levels separated by $\Delta m = 2$ and $\Delta m = 3$ are also possible, resulting in a total of six possible coherent oscillations. We named those transitions as one-photon, two-photon and three-photon transitions. Therefore, in this NMR device it is possible to observe six coherent transitions for each of the three nuclei (^{69,71}Ga and ^{75}As) in the point contact channel.

In order to observe the coherent oscillations, first the nuclear spin polarization is saturated and this is observed by resistance measurement, which is also saturated. Then pulsed rf magnetic field is applied by the antenna gate. If the frequency of the applied pulse is in resonance with the NMR frequency, oscillatory change in M_z is observed implying that the superposition coherently rotates between the two energy states. The oscillations in M_z is finally detected by the change in the resistance, ΔR_{xx}, before and after the application of the rf pulse. In Fig.2, NMR spectrum for one- and two- photon transitions are given only for ^{75}As. Coherent oscillations are observed for three-photon transitions, too (not shown here). In the same way, all of the six possible oscillations are observed for ^{69}Ga and ^{71}Ga [8].

The decoherence time T_2 of the device is estimated by curve fitting the coherent oscillation between $|-1/2\rangle$ and $|-3/2\rangle$ of ^{75}As. The T_2 was estimated as $\sim 0.6ms$ without any decoupling process. However, it is enhanced to $1.5ms$ when the nuclei-electron decoupling is applied [12]. The relaxation time T_1 in this device is longer than $100s$.

STATE MANIPULATIONS IN THE NANOSCALE NMR DEVICE

The four-level system in this device forms a quartit, which is equivalent to two logical qubits. This becomes clear if we identify $|0\rangle \equiv |00\rangle_{AB} \equiv |3/2\rangle$, $|1\rangle \equiv |01\rangle_{AB} \equiv |1/2\rangle$, $|2\rangle \equiv |10\rangle_{AB} \equiv |-1/2\rangle$, and $|3\rangle \equiv |11\rangle_{AB} \equiv |-3/2\rangle$ (see Fig. 2). Thus, the two-qubit state can be written as $|\psi\rangle = c_0|0\rangle + c_1|1\rangle + c_2|2\rangle + c_3|3\rangle$, where $\sum_i |c_i|^2 = 1$. In the following, we show how different quantum gate operations can be performed on this two fictitious qubit system by applying selective pulses at the resonant frequency between two energy levels, say $|m\rangle$ and $|n\rangle$. Here, the free evolution of the coherent system during the finite pulse duration and the time lag between the pulses are ignored, however they can be compensated during experimental realizations.

Rotations of logical qubit A in this quartit can be obtained by applying rf pulses at frequencies $\omega_0 - \Delta_q/\hbar$ and $\omega_0 + \Delta_q/\hbar$ two induce two-photon transitions: $\hat{X}_A(\theta) = \hat{X}_{02}(\theta)\hat{X}_{13}(\theta)$, $\hat{Y}_A(\theta) = \hat{Y}_{02}(\theta)\hat{Y}_{13}(\theta)$, and $\hat{Z}_A(\theta) = \hat{Z}_{02}(\theta)\hat{Z}_{13}(\theta)$, where $\hat{X}_{nm}(\theta), \hat{Y}_{nm}(\theta)$ and $\hat{Z}_{nm}(\theta)$ corresponds to rotations between levels $|m\rangle$ and $|n\rangle$ by an angle θ along the corresponding axes. In the same way, rotations on the logical qubit B can be obtained by applying pulses at frequencies $\omega_0 - 2\Delta_q/\hbar$ and $\omega_0 + 2\Delta_q/\hbar$ two induce one-photon transitions: $\hat{X}_B(\theta) = \hat{X}_{01}(\theta)\hat{X}_{23}(\theta)$, $\hat{Y}_B(\theta) = \hat{Y}_{01}(\theta)\hat{Y}_{23}(\theta)$, and $\hat{Z}_B(\theta) = \hat{Z}_{01}(\theta)\hat{Z}_{23}(\theta)$.

NOT Gate: The transformation of this two-qubit system when a NOT-gate is applied to the first (A) and second (B) logical qubits is described by $\hat{U}^A_{\rm NOT}|\psi\rangle = c_0|2\rangle + c_1|3\rangle + c_2|0\rangle + c_3|1\rangle$ and $\hat{U}^B_{\rm NOT}|\psi\rangle = c_0|1\rangle + c_1|0\rangle + c_2|3\rangle + c_3|2\rangle$, which can be implemented by the selective pulse sequences $\hat{U}^A_{\rm NOT} = i\hat{X}_{02}(\pi)\hat{X}_{13}(\pi)$ and $\hat{U}^B_{\rm NOT} = i\hat{X}_{01}(\pi)\hat{X}_{23}(\pi)$. On the other hand, NOT-gate

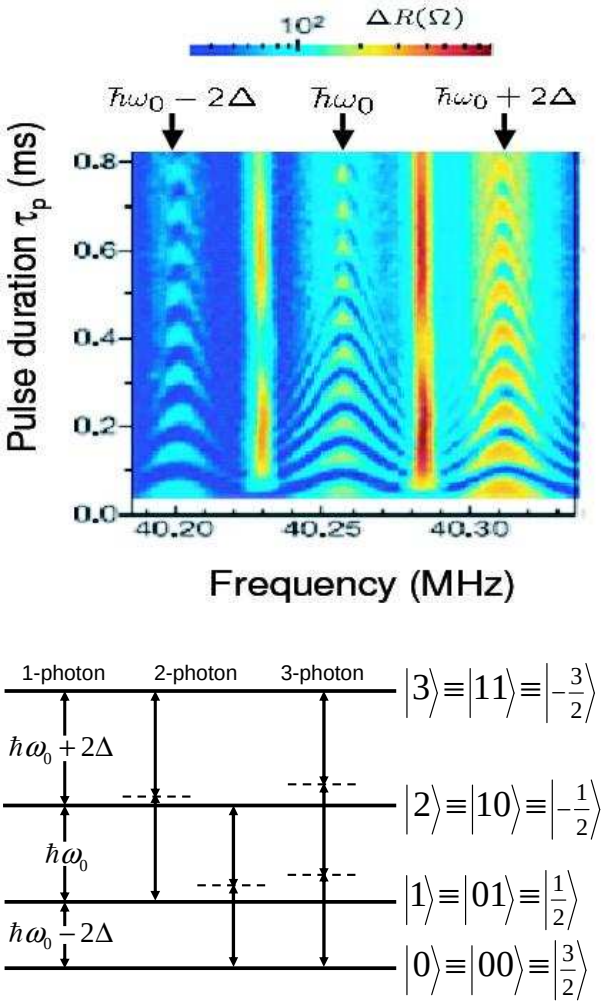

FIG. 2: Schematic energy level diagram of nuclear spin states for I=3/2 with electric quadrupolar interactions (lower figure) and coherent oscillations corresponding to single-photon and two-photon transitions between the four spin states observed for ^{75}As (upper). A three-photon transition was also observed for higher values of the alternating current through the antenna gate (data not shown). Measurements were performed at 100 mK with a magnetic field of 5.5T.

on both qubits can be obtained by a π-hard-pulse resulting in $\hat{U}^{AB}_{\rm NOT}|\psi\rangle = c_0|3\rangle + c_1|2\rangle + c_2|1\rangle + c_3|0\rangle$. One can easily see that $\hat{U}^{A}_{\rm NOT}$, which is implemented by pulses at two-photon transitions can be implemented by a hard-pulse followed by $\hat{U}^{B}_{\rm NOT}$.

Hadamard Gate: This truly quantum gate transforms the computational basis states into an equally weighted superposition states. A Hadamard operation on the first qubit makes the transformation $\hat{U}^{A}_{\rm H}|\psi\rangle = (c_0 + c_2)|0\rangle + (c_1 + c_3)|1\rangle + (c_0 - c_2)|2\rangle + (c_1 - c_3)|3\rangle$ and can be implemented by the pulse sequence $\hat{U}^{A}_{\rm H} = i\hat{Y}_{12}(\pi)\hat{X}_{01}(\pi)\hat{Y}_{01}(\pi/2)\hat{X}_{23}(-\pi)\hat{Y}_{23}(-\pi/2)\hat{Y}_{12}(-\pi)$. In the same way, Hadamard on the second qubit transforms the initial state as $\hat{U}^{B}_{\rm H}|\psi\rangle = (c_0 + c_1)|0\rangle + (c_0 - c_1)|1\rangle + (c_2 + c_3)|2\rangle + (c_2 - c_3)|3\rangle$ with the pulse sequence $\hat{U}^{B}_{\rm H} = i\hat{X}_{01}(\pi)\hat{Y}_{01}(\pi/2)\hat{X}_{23}(\pi)\hat{Y}_{23}(\pi/2)$.

CNOT Gate: In order to realize quantum algorithms on this NMR device, we should also show that effective realization of two-qubit operations are possible in this system. A CNOT gate with the first qubit as the control qubit and the second one as the target qubit is defined by the transformation $\hat{U}^{AB}_{\rm CNOT}|\psi\rangle = c_0|0\rangle + c_1|1\rangle + c_3|2\rangle + c_2|3\rangle$. On the other hand, the CNOT with the first qubit as the target and the second qubit as the control performs the transformation $\hat{U}^{BA}_{\rm CNOT}|\psi\rangle = c_0|0\rangle + c_3|1\rangle + c_2|2\rangle + c_1|3\rangle$. One can easily see that in this NMR device CNOT-like transformations can be implemented by just one pulse as $\hat{U'}^{AB}_{\rm CNOT} = \hat{Y}_{23}(\pi)$ and $\hat{U'}^{AB}_{\rm CNOT} = \hat{Y}_{13}(\pi)$. These gates differ from the ideal CNOT gate by an extra minus sign in one of the off-diagonal terms of the transformation matrix of the corresponding gate operation, i.e., $\hat{U'}^{AB}_{\rm CNOT}|\psi\rangle = c_0|0\rangle + c_1|1\rangle - c_3|2\rangle + c_2|3\rangle$. One can alternatively perform the same operations by applying $\hat{U}^{AB}_{\rm CNOT} = \hat{X}_{23}(\pi)$ and $\hat{U}^{AB}_{\rm CNOT} = \hat{X}_{13}(\pi)$. On the other hand, an ideal CNOT gate can be implemented by allowing a more complex sequence of one-photon transition pulses. As an example of this, we give the pulse sequence for $\hat{U}^{AB}_{\rm CNOT}$, which is $\hat{U}^{AB}_{\rm CNOT} = \hat{U}^{B}_{\rm H}\hat{Z}_{23}(\pi)\hat{Y}_{12}(-\pi)\hat{Z}_{23}(\pi/2)\hat{Z}_{01}(\pi/2)\hat{Y}_{12}(\pi)\hat{U}^{B}_{\rm H}$, where $\hat{U}^{B}_{\rm H}$ is defined as above. One may further simplify this pulse sequence by using combination of one- and two-photon transition pulses.

SWAP Gate: In principle, a swap gate, which employs the transformation $\hat{U}^{AB}_{\rm swap}|\psi\rangle = c_0|0\rangle + c_1|2\rangle + c_2|1\rangle + c_3|3\rangle$, can be implemented by a sequence of CNOT operations as follows $\hat{U}^{AB}_{\rm swap} = \hat{U}^{AB}_{\rm CNOT}\hat{U}^{BA}_{\rm CNOT}\hat{U}^{AB}_{\rm CNOT}$. On the other hand, for this device we can obtain SWAP-like gates by a single pulse $\hat{U}^{AB}_{\rm swap} = \hat{Y}_{12}(\pi)$ or $\hat{U}^{AB}_{\rm swap} = \hat{X}_{12}(\pi)$. This, too, differs from the ideal operation with a minus sign, which can be compensated by applying more complex pulse sequences.

Effective pure state preparation: For the correct working of the gate operations and consequently the quantum computer, NMR quantum computer should be properly prepared in an effective pure initial state of the nucleus ensemble. Contrary the conventional NMR, in our semiconductor NMR device we can prepare a large population available as the pure state. We owe this to the strongly polarized situation created due to dynamic nuclear spin polarization induced by the current flow. The initial state of the device is far from a pure state as schematically shown in 4. Note that due to dynamic polarization the population becomes larger for the higher spin states. From this initial state, one can apply $\hat{X}_{01}(\pi/2)\hat{X}_{12}(\pi)$ to prepare the $|11\rangle$. Once this state is prepared then we can prepare the pure state $|ij\rangle$ by applying the pulse $\hat{X}_{2i+j,3}(\pi)$ (see Fig. 4). More complicated pulse sequences allows us to prepare effective

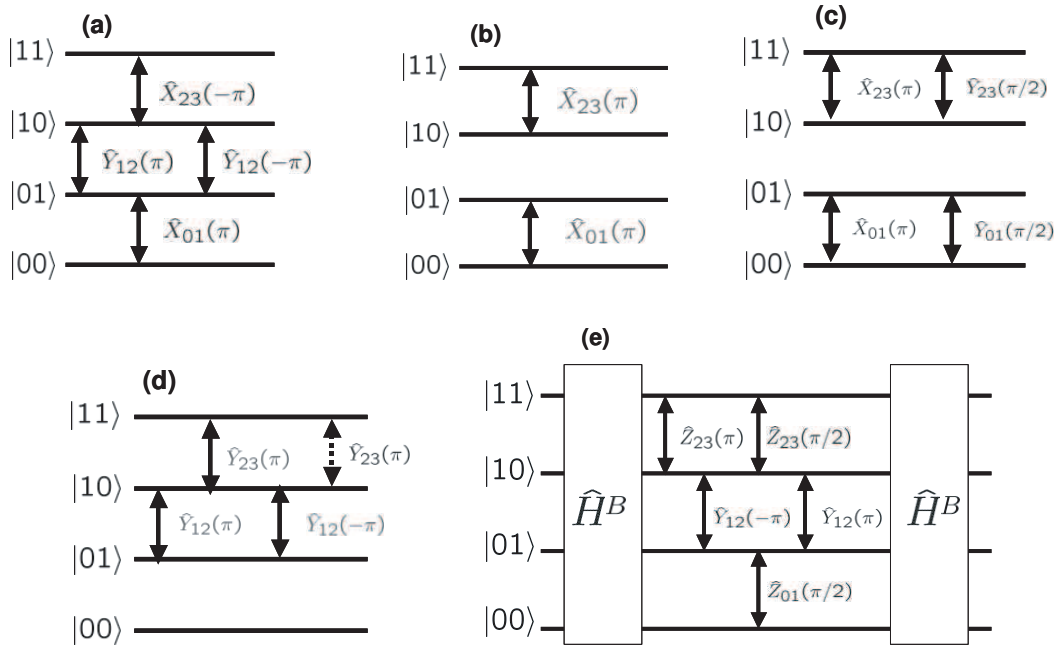

FIG. 3: Illustration of pulse sequences to realize (a) NOT gate on the first qubit A, (b) NOT gate on the second qubit B, (c) Hadamard gate on the second qubit B, (d) CNOT-like gate, and (e) ideal CNOT gate. In (d) the dotted (straight) arrow corresponds to the case when first (second) qubit is control and the second (first) qubit is target. In (e) $\hat{H}^B$ is the Hadamard gate illustrated in (c).

pure state from any arbitrary distribution. The designed population can be maintained up to T_1, which is longer than $100s$ for this device. Experimental results showing effective pure state preparation can be found in Ref. [12].

QUANTUM-STATE TOMOGRAPHY BASED ON M_z DETECTION

Quantum state tomography (QST) is a method for complete reconstruction of a given density matrix $\hat{\rho}$ in a serious of measurements. In general, to reconstruct completely a density matrix $\hat{\rho}$ for a quartit or two qubits, we need to determine 15 real parameters (The 16th element can be found from the normalization condition). Single NMR read-out can only give some of the either diagonal or off-diagonal elements of the given density matrix $\hat{\rho}$.

In case of the conventional NMR systems, where an M_{xy} measurement is performed, a single measurement gives directly some of the off-diagonal elements of the density matrix. However, in our NMR device, where an M_z measurement is employed, a single measurement determines only the population differences $\rho_{nn} - \rho_{mm}$ between the levels $|n\rangle$ and $|m\rangle$. This quantity is related to the diagonal elements of the density matrix, where $\rho_{mn} \equiv \langle m|\hat{\rho}|n\rangle$. In a typical NMR spectrum of our device peaks located at ω_{01}, ω_{12}, and ω_{23} give, respectively, $\rho_{11} - \rho_{00}$, $\rho_{22} - \rho_{11}$, and $\rho_{33} - \rho_{22}$. By imposing the normalization condition, we can easily obtain the diagonal elements ρ_{ii} of the density matrix. The remaining elements of the density matrix can be obtained by rotating the original density matrix by properly chosen rotation operations $\hat{R}_k$, which transform the original matrix into $\hat{\rho}_k = \hat{R}_k \rho \hat{R}_k^\dagger$. These rotations move the off-diagonal elements of the original density matrix to the diagonal of the rotated density matrix so that M_z measurement provides information on them. By application of a number of such rotations, the off-diagonal elements of the density matrix can be brought into the measurable ones in M_z detection. The set of $\hat{R}_k$ operations is not unique, one can find many different sets of rotations for complete reconstruction of the density matrix using M_z detection. We found that the following set of 12 rotations is suitable for the reconstruction of the density matrix using M_z detection based state tomography for our device

$$\begin{array}{lll} \hat{R}_1 = \hat{X}_{01}(\pi/2), & \hat{R}_2 = \hat{Y}_{01}(\pi/2), & \hat{R}_3 = \hat{X}_{12}(\pi/2), \\ \hat{R}_4 = \hat{Y}_{12}(\pi/2), & \hat{R}_5 = \hat{X}_{23}(\pi/2), & \hat{R}_6 = \hat{Y}_{23}(\pi/2), \\ \hat{R}_7 = \hat{X}_{02}(\pi/2), & \hat{R}_8 = \hat{Y}_{02}(\pi/2), & \hat{R}_9 = \hat{X}_{13}(\pi/2), \\ \hat{R}_{10} = \hat{Y}_{13}(\pi/2), & \hat{R}_{11} = \hat{X}_{03}(\pi/2), & \hat{R}_{12} = \hat{Y}_{03}(\pi/2). \end{array} \quad (1)$$

One can optimize the rotation set to decrease the number of rotations and/or increase the reconstruction sensitivity. The following is one of such a set composed only of six operations and still exhibiting high scheme sensitivity parameter. The rotations in this set are

$$\hat{R}_1 = \hat{X}_{01}(\pi/2)\hat{X}_{23}(\pi/2),$$

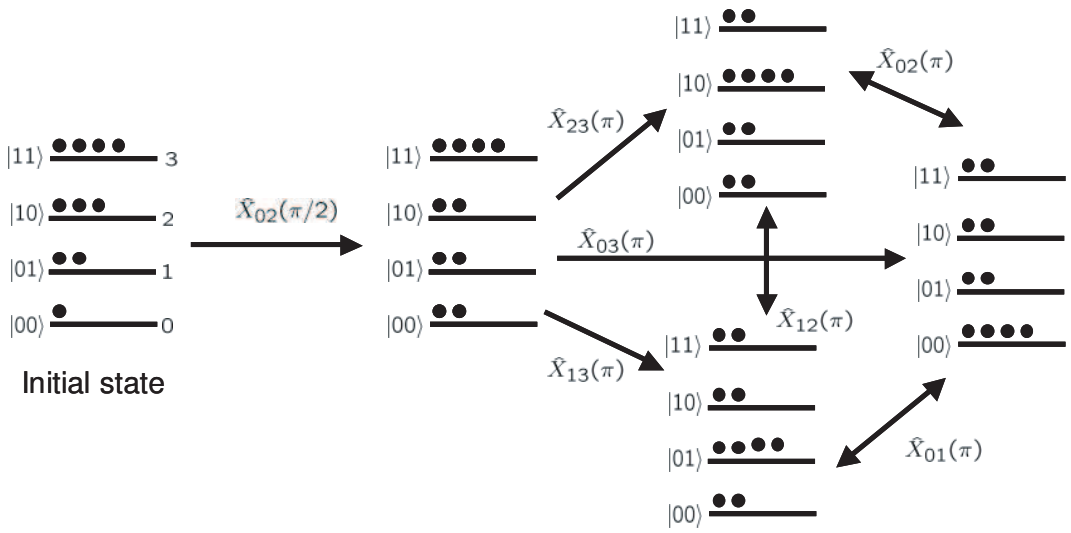

FIG. 4: A schematic illustration of pulse sequences for effective pure state preparation starting from the initial state of the semiconductor NMR device. Note that two-photon and three-photon transitions can be decomposed into one-photon transitions using more complicated pulse sequences, i.e, $X_{02}(\pi/2) = X_{01}(\pi/2)X_{12}(\pi)$.

$$
\begin{aligned}
\hat{R}_2 &= \hat{Y}_{01}(\pi/2)\hat{Y}_{23}(\pi/2), \\
\hat{R}_3 &= \hat{X}_{01}(\pi/2)\hat{Y}_{13}(\pi)\hat{X}_{12}(\pi/2), \\
\hat{R}_4 &= \hat{Y}_{01}(\pi/2)\hat{Y}_{13}(\pi)\hat{Y}_{12}(\pi/2), \\
\hat{R}_5 &= \hat{X}_{02}(\pi/2)\hat{X}_{13}(\pi/2), \\
\hat{R}_6 &= \hat{Y}_{02}(\pi/2)\hat{Y}_{13}(\pi/2)
\end{aligned}
\tag{2}
$$

CONCLUSIONS

All-electrical coherent control of nuclear spins in a nanoscale NMR chip has been demonstrated. Clear coherent oscillations reflect all possible transitions among the four nuclear spin states of each of the nuclide (^{69,71}Ga and ^{75}As) in the point contact channel. Since arbitrary control of superpositions among the four spin levels can be performed in this device, one and two qubit operations are possible. We have theoretically shown how to utilize this four-level system as a fictitious two-qubit system, and designed the pulse sequences for the realization of one- and two-qubit quantum operations. Moreover, we proposed an NMR state tomography scheme based on the detection of longitudinal magnetization of the nuclear spins.

Although we have not shown in this manuscript, we performed preliminary experiments [12] for the preparation of effective pure states, which are important for the initialization of the NMR quantum computer. Dynamic nuclear spin polarization induced by the current flow allowed us to prepare a large population to use for the preparation of effective pure states.

The results shown in this paper suggest that this nanometre-scale NMR device is a good candidate for quantum-information processing based on solid-state systems.

Acknowledgments. ŞKO and AM kindly acknowledge support from the Japan Society for the Promotion of Science within the 21st Century COE Program. AM also acknowledges grant No. 1 P03B 064 28 of the Polish KBN.

[1] D. G. Cory, A. F. Fahmy and T. F. Havel, PNAS USA **94**, 1634 (1997).
[2] N. Gershenfeld and I. L. Chuang, Science **275**, 350 (1997).
[3] L. M. K. Vandersypen and I. L. Chuang, Rev. Mod. Phys. **76**, 1037 (2004).
[4] D. G. Cory *et al.*, Fortschr. Phys. **48**, 875 (2000).
[5] B. E. Kane, Nature **393**, 133 (1999).
[6] T. D. Ladd, J. R. Goldman, F. Yamaguchi, Y. Yamamoto, E. Abe, and K. M. Itoh, Phys. Rev. Lett. **89**, 017901 (2002).
[7] H. Kampermann, and W. S. Veeman, J. Chem. Phys. **122**, 214108 (2005).
[8] G. Yusa, K. Muraki, K. Takashina, K. Hashimoto, and Y. Hirayama, Nature **434**, 1001 (2005).
[9] S. Kronmuller, W. Dietsche, K. von Klitzing, G. Denninger, W. Wegscheider, and M. Bichler, Phys. Rev. Lett. **82**, 4070 (1999).
[10] K. Hashimoto, K. Muraki, T. Saku, and Y. Hirayama, Phys. Rev. Lett. **88**, 176601 (2002).
[11] J. H. Smet, R. A. Deutschmann, F. Ertl, W. Wegscheider, G. Abstreiter, and K. von Klitzing, Nature **415**, 281 (2002).
[12] Y. Hirayama, A. Miranowicz, T. Ota, G. Yusa, K. Muraki, Ş. K. Özdemir, and N. Imoto, J. Phys.: Condens. Matter **18**, S885 (2006).